

The different roles of Pu-oxide overlayers in the hydrogenation of Pu-metal: An *ab initio* molecular dynamics study based on vdW-DFT+ U

Bo Sun,* Haifeng Liu, Haifeng Song, Guangcai

Zhang, Hui Zheng, Xian-Geng Zhao, and Ping Zhang†

Institute of Applied Physics and Computational Mathematics, Beijing 100094, P.R. China

Abstract

Based on the van der Waals density functional theory (vdW-DFT)+ U scheme, we carry out the *ab initio* molecular dynamics (AIMD) study of the interaction dynamics for H_2 impingement against the stoichiometric $PuO_2(111)$, the reduced $PuO_2(111)$, and the stoichiometric α - $Pu_2O_3(111)$ surfaces. The hydrogen molecular physisorption states, which can not be captured by pure DFT+ U method, are obtained by employing the vdW-DFT+ U scheme. We show that except for the weak physisorption, $PuO_2(111)$ surfaces are so difficult of access that almost all of the H_2 molecules will bounce back to the vacuum when their initial kinetic energies are not sufficient. Although the dissociative adsorption of H_2 on $PuO_2(111)$ surfaces is found to be very exothermic, the collision-induced dissociation barriers of H_2 are calculated to be as high as 3.2 eV and 2.0 eV for stoichiometric and reduced PuO_2 surfaces, respectively. Unlike PuO_2 , our AIMD study directly reveals that the hydrogen molecules can penetrate into α - $Pu_2O_3(111)$ surface and diffuse easily due to the 25% native O vacancies located along the $\langle 111 \rangle$ diagonals of α - Pu_2O_3 matrix. By examining the temperature effect and the internal vibrational excitations of H_2 , we provide a detailed insight into the interaction dynamics of H_2 in α - Pu_2O_3 . The optimum pathways for hydrogen penetration and diffusion, the corresponding energy barriers (1.0 eV and 0.53 eV, respectively) and rate constants are systematically calculated. Overall, our study fairly reveals the different interaction mechanisms between H_2 and Pu-oxide surfaces, which have strong implications to the interpretation of experimental observations.

PACS numbers: 68.35.Ja, 71.15.Pd, 71.27.+a, 82.65.Pa

*sun_bo@iapcm.ac.cn

†zhang_ping@iapcm.ac.cn

I. INTRODUCTION

Plutonium (Pu) is one kind of strategically vital fissile material owning attractive nuclear properties for both energy production and nuclear explosives. From basic point of view, Pu is the most complex element in the periodic table showing such intricate properties as the complicated Pu-5*f* states [1–4], which are very sensitive to the slight variations of the surrounding physical and chemical environments. Thus, since it was first isolated and the samples became available, Pu has always been challenging the boundaries of knowledge of the fundamental science and attracting extensive researching attentions. However, during the preparation/handling of Pu-sample and the long-term storage of Pu-device, the reactive Pu metal will easily suffer from the environment-dependent chemical corrosions, among which the surface oxidation is to some extent unavoidable because of the ubiquitous oxygen in the realistic environment. Also, the surface hydrogenation is catastrophic for Pu and need to be avoided since the Pu-hydride product can violently catalyze the oxidation (by a factor of 10^{13}) and even induce the pyrophoricity of Pu. Actually, the surface corrosion and oxidation of Pu are often treated as equivalent topics since the readily generated surface layers of Pu oxides prominently influence other corrosion courses of Pu metal such as the first step of Pu-hydrogenation named the induction period. Moreover, given the high radioactivity and toxicity of Pu, the easily dispersed Pu-hydride and Pu-oxide undoubtedly bring more hazards to the personnel and the environment during handling and storage of Pu metal. Therefore, understanding the effects of Pu-oxide surface layers in the chemical corrosion (especially the hydrogenation) of Pu metal is crucial for the plutonium science, the environment, and the nuclear energy sectors. However, it is also full of challenges that beset experimentalists.

As a matter of fact, the oxidized surface layers are directly involved in the corrosion process of Pu metal. In many technological applications of Pu oxides such as in nuclear fuel cycle, it is always desirable to study the surface properties and surface reactivity of Pu oxides. Many experiments [5–7] have been devoted to studying the oxidation mechanisms of Pu metal under various atmospheres and temperatures, and eventually come to a main conclusion that the multivalent nature of Pu presents an active response to the varying environment, in other words, it is difficult to stabilize Pu at one oxidation state when the surrounding conditions (such as relative humidity, oxygen content, and the temperature) change. As a result, the complex Pu-O phase diagram [8] has not been completely described

yet, let along the detailed surface conditions of such many kinds of Pu oxides. When exposed to oxygen-rich air, metallic Pu surface oxidizes to a protective dioxide (PuO_2) layer [6, 7, 9] and a thin sesquioxide (Pu_2O_3) layer existing in between. Under special aqueous condition, the hydration reaction on PuO_2 surfaces ($\text{PuO}_2 + x\text{H}_2\text{O} \rightarrow \text{PuO}_{2+x} + x\text{H}_2$) has been reported to generate higher compound PuO_{2+x} ($x \leq 0.27$) [10]. Whereas, it has been theoretically proved to be strongly endothermic [11] and the products (PuO_{2+x}) have been experimentally found to be chemically unstable at elevated temperatures [12]. Thus, PuO_2 is the stable oxide as the compound of choice for the long-term storage of Pu and as the nuclear fuels. However, under oxygen-lean conditions (in the vacuum or inert gas), the PuO_2 -layer undergoes the thermodynamically driven auto-reduction (AR) to Pu_2O_3 , including the low-temperature phase of α - Pu_2O_3 in cubic structure ($Ia\bar{3}$) and the high-temperature β - Pu_2O_3 in a hexagonal structure ($P\bar{3}m1$). More recently, sub-stoichiometric sesquioxide $\text{Pu}_2\text{O}_{3-y}$ ($y = 0$ to 1) has been obtained from further AR of PuO_2 layer on Pu surface [13]. All of those studies have shown us the complex surface conditions of oxide-coated Pu, and made us believe that they are one of the controlling factors for the subsequent corrosion of Pu. As pointed out hereinbefore, for the safe handling and storage of Pu-based materials, it is a very important topic to control or avoid the catastrophic Pu-hydrogenation. Whereas, early experiments have found that the length of induction period in Pu-hydrogenation is mainly determined by the component and configuration of the preexisting Pu-oxide overlayer, namely, compared with the PuO_2 overlayers under ambient conditions, the Pu_2O_3 under ultra high vacuum (UHV) conditions can promote the Pu-hydrogenation reaction by markedly shortening the induction period [6]. Since then, experimentalists have invested persistent efforts to better understand the roles of Pu-oxide overlayers and to quantify the controlling factors/parameters in detail [14], aiming to establish a predictive model of Pu-hydrogenation. More recently, Dinh *et al.* [15] have investigated the role of cubic α - Pu_2O_3 in the hydrogenation of PuO_2 -coated Pu by chemically and mechanically altering the PuO_2 surface on Pu, and demonstrated that induction periods are consistently eliminated at conditions that produce catalytic α - Pu_2O_3 . They also pointed out that more experimental efforts are surely needed to clarify such unclear factors for the unpredictable induction period as the solubility and diffusion of hydrogen species in Pu oxides. McGillivray *et al.* [16] have determined hydrogen pressure (P_{H_2}) dependence of two early steps (namely, induction and nucleation) of Pu-hydrogenation reaction by synthesizing a well reproducible PuO_2 overlayer. They found that the induction

time and the nucleation rate vary inversely and linearly with P_{H_2} , respectively. From their standpoint, the diffusion barrier properties of hydrogen in PuO_2 are not sensitive to the temperature (cooling from 150 to 25 °C) and the oxygen content (varying from vacuum to O-rich) during the PuO_2 synthesis. Although all experimental studies so far have definitely demonstrated the distinct roles of PuO_2 and $\alpha\text{-Pu}_2\text{O}_3$ overlayers, such details as the interaction mechanisms of molecular H_2 with Pu-oxide surfaces and the diffusion behaviors of hydrogen species in Pu oxides have not been clarified, and demand further study from a very fundamental viewpoint. However, given the complexity and hazard listed above, it is extraordinarily difficult to experimentally clarify what happens in the early stages when the H_2 molecules are either physisorbed or chemisorbed, and subsequently the H_2 either dissociate to create reactive species or diffuse into the Pu-oxide overlayers. Thus, the atomic simulations are highly required for the in-depth understanding of the interaction dynamics of H_2 molecule with Pu-oxide overlayers.

In order to address the above-mentioned issues, theoretical schemes have to reasonably describe the ground state properties of Pu oxides at first, and then guarantee that the *ab initio* molecular dynamics (AIMD) simulations of the interactions between Pu-oxide surfaces and H_2 molecules are methodologically reliable and computationally viable. However, the conventional density-functional theory (DFT) underestimates the strong on-site Coulomb repulsion of the $5f$ electrons and incorrectly describes PuO_2 as a metal [17] instead of a Mott insulator reported by experiments [18]. Fortunately, several beyond-DFT approaches, including the DFT+ U [19], the self-interaction corrected LDA [2, 20], the hybrid density functional of (Heyd, Scuseria, and Enzerhof) HSE [21], and LDA+dynamical mean-field theory (DMFT) [22], have been developed to correct the failures of conventional DFT in calculations of Pu oxides. The effective modification of the pure DFT by the DFT+ U formalism has been confirmed widely in studies of physical properties of Pu-oxides (PuO_2 , $\alpha\text{-Pu}_2\text{O}_3$ and $\beta\text{-Pu}_2\text{O}_3$) [23–32], such as the insulating ground states, the lattice parameters, the bulk modulus, the phonon spectra and density of states (DOS), the surface stability and chemical activity, and the redox energetics. Note that within the DFT+ U framework, both PuO_2 and Pu_2O_3 are described as the antiferromagnetic (AFM) insulator. The calculated AFM ground state of Pu_2O_3 is actually consistent with experimental measurements [33, 34]. However, unlike the affirmative AFM Pu_2O_3 and UO_2 , PuO_2 is peculiar due to its complex ground-state multiplet, so that strictly speaking its paramagnetic ground state has not

been well understood and an AFM exchange [35, 36] between Pu ions in PuO₂ is still used to explain the discrepancy between neutron-scattering experiments [37] and magnetic susceptibility measurements [38], which is beyond the scope of our current work. In spite of all the published papers and increasing attentions focusing on Pu oxides, our theoretical understanding on the basic mechanisms for the hydrogenation of Pu-oxide coated Pu is, to put it mildly, very poor. Especially, little is known regarding the interaction behaviors of H₂ on Pu-oxide surfaces, which is in sharp contrast to the depth and comprehensiveness of researches conducted upon the surface reaction mechanisms of ceria [39–44]. As far as we are aware, Wu *et al.* [26, 27] were the only ones who have studied the interaction between gaseous molecule (H₂O) and PuO₂(100)/PuO₂(110) surfaces, whereas in their literature both the strong correlation effect of Pu-5*f* electrons and the van der Waals force between polar H₂O molecule and PuO₂ surfaces were not taken into account. Recently, Jomard and Bottin [30] have via DFT (PBE)+*U* calculations discussed the influence of electronic correlations on thermodynamic stability of PuO₂ surfaces and pointed out that the O-terminated PuO₂(111) is the most stable surface and DFT+*U* method can well describe the electronic structure of the insulating PuO₂ surfaces, which is a prerequisite to study surface reactivity of PuO₂. In order to thoroughly understand the surface properties of PuO₂, we have discussed the effects of thickness and O-vacancy on surface stability and chemical activity of PuO₂ based on the DFT+*U* formalism with the spin-orbit coupling (SOC) effect included, and found that under O-rich conditions, the stoichiometric O-terminated PuO₂(111) surface is thermodynamically stable and chemically inert, while the O-reducing condition facilitates the formation of on-surface O-vacancy, which is expected to enhance the chemical activities of PuO₂(111) surface [31].

As a continuation of our theoretical studies on Pu-surface corrosion [31, 32], in this paper, we study the interaction dynamics of H₂ molecule with Pu-oxide surfaces to clarify the different roles of PuO₂ and α -Pu₂O₃ overlayers in the hydrogenation of Pu-metal. Specifically, based on the systematic simulations within the vdW-DFT+*U* framework, we address the following issues: (i) the interaction behaviors such as adsorption, collision, and dissociation of a cold or hot H₂ on stoichiometric and reduced PuO₂(111) surfaces; (ii) the interaction between H₂ and stoichiometric α -Pu₂O₃(111) surface and the kinetic energy-dependent penetration of H₂ into α -Pu₂O₃(111) overlayer; (iii) the adsorption and diffusion behaviors of H₂ in the α -Pu₂O₃ matrix, and the interaction between the H₂ of vibrational excitation and

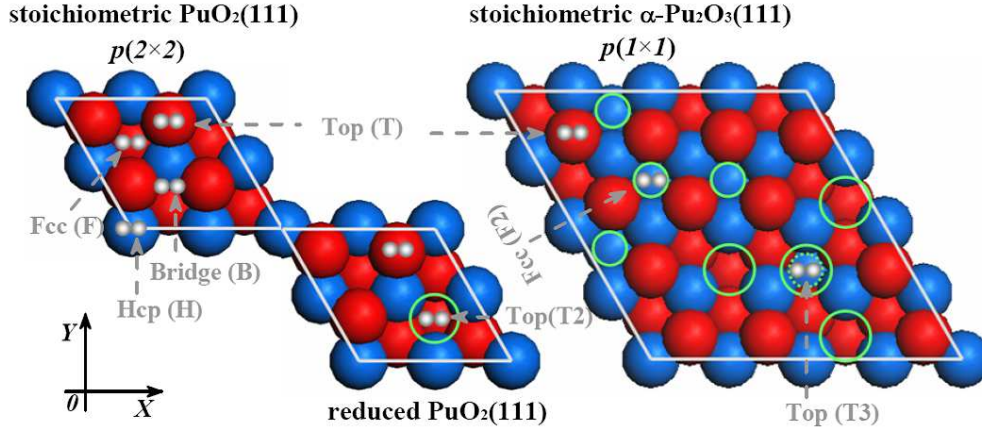


FIG. 1: (Color online). Top views of Pu-oxide surface configurations: the $p(2 \times 2)$ stoichiometric $\text{PuO}_2(111)$ and reduced $\text{PuO}_2(111)$ surfaces, and the $p(1 \times 1)$ stoichiometric $\alpha\text{-Pu}_2\text{O}_3(111)$ surface, where the high-symmetry target sites for H_2 molecule are also labeled. The blue, red and dark grey spheres denote Pu, O and H atoms, respectively. The visible O vacancies on the first, the second and the third oxygen layers are marked by big solid, small solid and small dashed green circles, respectively.

the $\alpha\text{-Pu}_2\text{O}_3$ during the diffusion. The rest of this paper is organized as follows. The details of our calculations are described in Sec. II. In Sec. III we present and discuss the results. In Sec. IV, we summarize our main conclusions.

II. DETAILS OF CALCULATION

The spin-polarized vdW-DFT+ U calculations are performed using the Vienna *ab initio* simulation package (VASP) [45] with the projector-augmented wave (PAW) method [46] and a plane-wave cutoff energy of 400 eV. The Pu- $6s^27s^26p^66d^25f^4$, O- $2s^22p^4$, and H- $1s^1$ electrons are treated as valence electrons, while the remaining electrons were kept frozen as core states in the PAW method. The electronic exchange and correlation are treated within the generalized-gradient approximation (GGA) using the Perdew-Burke-Ernzerhof (PBE) functional [47], and the strong on-site Coulomb repulsion among the Pu- $5f$ electrons is described with the DFT+ U scheme formulated by Dudarev *et al.* [19]. Thus, in this study a Hubbard U -like term ($U_{eff}=U-J$, i.e. the difference between the Coulomb U and exchange J parameters, hereinafter referred to as U) is added to the PBE functional. In

the previous DFT+ U studies of PuO_2 , the choices of U and J parameters are based on an overall agreement between available experimental data and theoretical results as regarding the basic physical properties of the ground state, and the combination of $U=4.75$ and $J=0.75$ eV has been proved to be reasonable by our previous calculations [23–25, 28, 31, 32] of PuO_2 and Pu_2O_3 . Furthermore, the DFT+ U method has been shown to give substantially similar results to those obtained by hybrid functionals [21] with partial exact exchange. Note that the computational demand of DFT+ U is close to that of conventional LDA or GGA functionals and much less than that of hybrid functionals, which are computationally too time-consuming to do the AIMD simulations of such surface systems as studied in this paper.

The Pu-oxide surfaces are modeled by finite-sized periodic slab supercells, consisting of a number of oxide layers infinite in X and Y directions and separated in the Z direction by a vacuum of 30 Å, which is found to sufficiently minimize the interaction between adjacent slabs. Following our previous DFT+ U studies of PuO_2 surfaces [31], in this work we first calculate the surface energy E_s^{relax} of the stoichiometric $\alpha\text{-Pu}_2\text{O}_3$ slabs. This quantity is written as

$$E_s^{\text{relax}} = \frac{1}{2A} (E_{\text{slab}}^{\text{relax}} - E_{\text{bulk}}), \quad (1)$$

where $E_{\text{slab}}^{\text{relax}}$ is the total energy of the fully relaxed $\alpha\text{-Pu}_2\text{O}_3$ surface slab, E_{bulk} is the energy of the reference bulk $\alpha\text{-Pu}_2\text{O}_3$ with the same number of atoms, and the denominator $2A$ is the total area of both surfaces of the slab with a finite thickness. Based on extensive test calculations, the E_s^{relax} of a slab with varying thickness is found to be converged within 5 meV/Å². According to Tasker’s general criteria [48] on surface stability of an ionic crystal, the O-terminated $\alpha\text{-Pu}_2\text{O}_3(111)$ slab, consisting of successive and electrically neutral “O-Pu-O” blocks along the Z direction, has the “Tasker-type-II” surfaces and its surface energy E_s^{relax} is calculated to be ~ 0.03 eV/Å². The $\alpha\text{-Pu}_2\text{O}_3(110)$ is the typical “type-I” surface stacked with identical neutral planes fulfilling the $\alpha\text{-Pu}_2\text{O}_3$ stoichiometry with its E_s^{relax} of ~ 0.07 eV/Å². The polar “type-III” (001) surface, consisting of oppositely charged planes, is in this work modeled as two oxygen-terminated surfaces with 50% oxygen vacancies to fulfill the stoichiometric formula and to quench the dipole moment of the repeated unit in Z direction, and its E_s^{relax} is found to be the largest one (~ 0.23 eV/Å²). Thus, for both PuO_2 and $\alpha\text{-Pu}_2\text{O}_3$, the O-terminated (111) surface is most stable and is briefly named as the (111) surface if not mentioned differently in this study.

Considering the auto-reduction (AR) of PuO_2 to $\alpha\text{-Pu}_2\text{O}_3$ driven by the oxygen reducing/poor conditions, in this study, we therefore mainly study three model surfaces of Pu-oxides, corresponding to three typical cases of varying oxygen conditions, namely, stoichiometric/ideal $\text{PuO}_2(111)$ surface (oxygen rich condition), reduced/defective $\text{PuO}_2(111)$ surface with 25% O vacancies (oxygen reducing), and stoichiometric $\alpha\text{-Pu}_2\text{O}_3(111)$ surface (oxygen poor). The top views of $p(2 \times 2)$ stoichiometric and reduced $\text{PuO}_2(111)$ surfaces and $p(1 \times 1)$ stoichiometric $\alpha\text{-Pu}_2\text{O}_3(111)$ surface used in the calculations are shown in Fig. 1. The Brillouin zone (BZ) integration is performed using the Monkhorst-Pack (MP) k -point mesh [49]. Specifically, for both stoichiometric and reduced $\text{PuO}_2(111)$ surfaces, the two-dimensional (2D) $p(2 \times 2)$ cell with a $7 \times 7 \times 1$ k -point MP grid is employed in the static calculations, and a $3 \times 3 \times 1$ k -point MP grid is used in AIMD simulations. Since the ideal stoichiometric $\alpha\text{-Pu}_2\text{O}_3$ is structurally similar to the $2 \times 2 \times 2$ fluorite PuO_2 ($Fm\bar{3}m$) supercell containing 25% O vacancy located in the $16c$ (0.25, 0.25, 0.25) sites, the surface area of unit $p(1 \times 1)$ $\alpha\text{-Pu}_2\text{O}_3(111)$ cell is equal to that of the $p(4 \times 4)$ $\text{PuO}_2(111)$ cell. Thus, a $3 \times 3 \times 1$ k -point MP grid is used in static calculations and it is restricted to the Γ -point in AIMD simulations. The slab of $p(2 \times 2)\text{-PuO}_2(111)$ consists of 6 “O–Pu–O” blocks along the Z direction, including totally 24 plutonium and 48 oxygen atoms, and the $\alpha\text{-Pu}_2\text{O}_3(111)$ surface model contains 4 “O–Pu–O” blocks with 64 Pu and 96 O atoms in the supercell. In the spin-polarized static calculations of Pu-oxide slabs with the AFM orders of the Pu-sublattice set to be in a simple “ $\uparrow \downarrow \uparrow \downarrow$ ” alternative manner along the Z direction, the two “O–Pu–O” oxide bottom blocks are fixed to their calculated bulk positions ($a_{\text{PuO}_2} = 5.466 \text{ \AA}$ and $a_{\alpha\text{-Pu}_2\text{O}_3} = 11.20 \text{ \AA}$) and all other atoms are fully relaxed until the Hellmann-Feynman forces become less than 0.01 eV/\AA . The dipole-dipole interactions along the direction perpendicular to the slab are also corrected, as implemented in the VASP code [50, 51].

Due to the “Tasker-type-II” character of $\text{PuO}_2(111)$ and $\alpha\text{-Pu}_2\text{O}_3(111)$ surfaces, the non-coplanar O-anion and Pu-cation may generate surface dipole moment along the Z direction, especially when the surface O-vacancies exist. In order to detailedly discuss the multiple interaction mechanisms between H_2 and Pu-oxide surfaces, van der Waals (vdW) dispersion forces upon H_2 had better be considered. In this study, we employ the non-local vdW-DFT+ U approach [52, 53] to calculate the static potential-energy pathway (PEP) along which a cold H_2 approaches to Pu-oxide surfaces, and to simulate the dynamic interaction

between a hot H₂ (with certain initial kinetic energy) and the Pu-oxide surfaces. Moreover, we expect that the static PEP calculations and the AIMD simulations can complement each other to achieve a thorough understanding of the energetics factor and dynamics process determining the distinct roles of PuO₂ and α -Pu₂O₃ overlayers in Pu hydrogenation. From the PEP results, we can analyze the binding strength between Pu-oxide and H₂ molecule via the adsorption energy E_{ad} , which is given by

$$E_{\text{ad}} = E_{\text{H}_2/\text{Pu-oxide}} - (E_{\text{Pu-oxide}} + E_{\text{H}_2}). \quad (2)$$

Here, $E_{\text{H}_2/\text{Pu-oxide}}$, $E_{\text{Pu-oxide}}$ and E_{H_2} are the total energies of the adsorption system, the pure Pu-oxide system, and the H₂ molecule without zero-point vibration, respectively.

The AIMD simulations under the Born-Oppenheimer approximation are performed using the Verlet algorithm with a time step of 0.5 fs within the micro canonical ensemble (NVE). With the NVE-AIMD, the very fast impingement of H₂ molecule against the Pu-oxide surfaces is simulated to uncover the possible molecular dissociation and estimate the high dissociation barriers. Based on the harmonic approximation and the vibrational energy E_{vib} written as

$$E_{\text{vib}} = \left(\frac{1}{2} + n\right)h\nu, \quad (3)$$

the ground-state zero-point vibration ($n = 0$) and internal vibrational excitation ($n = 1$ or 2) of H₂ molecule with a calculated harmonic frequency ($\nu = 128$ THz) are also considered. In addition, the canonical ensemble (NVT) at several prefixed temperatures through a Nosé thermostat [54] has also been employed as an alternative approach to discuss the high temperature effect on the state or behavior of H₂ molecule in α -Pu₂O₃. However, the short time scale that can be simulated by the AIMD based on vdW-DFT+ U is a major limitation for such rare events as the penetration and diffusion of H₂ molecule in this study, which usually take place on a much longer timescale (of milliseconds or more) than the atomic vibrational timescale of femtoseconds. Here, we attempt to depict such rare events by using the harmonic transition state theory (hTST) with the rate constant given by

$$k_{\text{hTST}}^{\text{Pen/Diff}} = \frac{\prod_i^{3N} \nu_i^{\text{IS}}}{\prod_i^{3N-1} \nu_i^{\text{TS}}} e^{-\Delta E/k_B T}, \quad (4)$$

where ν_i^{IS} and ν_i^{TS} are the normal mode vibrational frequencies of the initial and transition states, respectively. Here, the energy barrier ΔE is defined as the energy difference between the initial state (IS) and transition state (TS), where the TS structures for relevant processes

are located by employing the climbing image nudged elastic band (CI-NEB) method [55] using at least three images along each pathway. The vibrational frequencies are obtained by diagonalization of the force-constant matrix in Cartesian coordinates (Hessian), where the force constants are obtained from finite differences of the forces with atomic displacements of ± 0.02 Å. Then, we can further use the frequencies to characterize whether an optimized stationary point is an initial/minimum state without imaginary frequency or a TS with only one imaginary frequency.

III. RESULTS AND DISCUSSION

Since the surface interaction with molecular monomer is very site-specific, as shown in Fig. 1, in this study we consider four high-symmetry target sites (T1, H1, F1, and B1) for a H_2 molecule approaching the stoichiometric $PuO_2(111)$ surface, and also four sites (T1, T2, H1, and H2) on the reduced $PuO_2(111)$ surface with an artificial surface oxygen vacancy marked by a solid green circle in Fig. 1. For the stoichiometric $\alpha\text{-}Pu_2O_3(111)$ surface shown in Fig. 1, where the visible O vacancies on the first/outmost, the second/subsurface, and the third/deep oxygen layers are marked by big solid, small solid, and small dashed green circles, respectively, we consider three adsorption sites (T1, T3, and F2). Due to the 25% O vacancies existing inherently in $\alpha\text{-}Pu_2O_3$, one can see that T3 is actually a special site, under which two superposed O vacancies seem to bore a hole in the $\alpha\text{-}Pu_2O_3(111)$ slab and may act as an entrance for the smallest diatomic molecule H_2 with its bond-length of only 0.75 Å.

The H_2 molecule is initially placed over different Pu-oxide surface sites with a height of 4 or 4.5 Å and the initial orientation at each site is set to be along the X , Y , and Z axes, respectively. Altogether, we construct 33 high-symmetry initial geometries of H_2 on three Pu-oxide surfaces and name them by adding a corresponding postfix—T1- X for example, among which 11 ‘- X ’ structures are presented in Fig. 1. In addition, we also generate some low-symmetry initial geometries by rotating H_2 with small angles, and find that low-symmetry geometries can relax into the high-symmetry ones after geometry optimization. Thus, in the static PEP calculations, the H-H bond is fixed to be either parallel or perpendicular (i.e., the ‘- Z ’ cases) to the (111) surface when the H_2 molecule drops step by step from its initial location. Since a H_2 molecule on a solid surface has 6 degrees of freedom

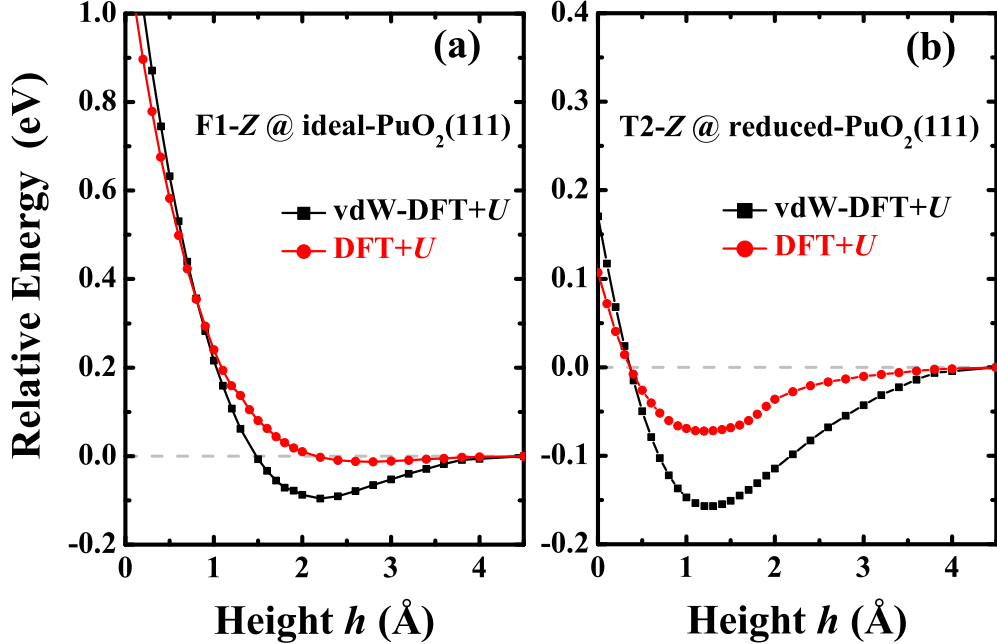


FIG. 2: (Color online) Calculated PEPs of the H_2 molecule approaching (a) the ideal- $\text{PuO}_2(111)$ surface from the initial F1- Z geometry; and (b) the reduced- $\text{PuO}_2(111)$ from T2- Z . The initial geometries with $h_0 = 4.5 \text{ \AA}$ are considered as the reference systems, with their total energies set to 0 eV.

(6-DOF) [see the inset to Fig. 3(e), i.e., bond-length d , height h , azimuth angles (θ and ϕ) of H_2 , and projected positions (X , Y) of mass center], so that in the static PEP calculations we consider in practice 5-DOF of H_2 except for θ . However, during the AIMD simulations of the H_2 molecule with a given kinetic energy E_k^\perp impingement against the initially resting/cold Pu-oxide surface, we let both the molecule and the surface layers relax freely.

A. The interaction between H_2 and $\text{PuO}_2(111)$ surfaces

In this subsection, we focus on the interaction mechanisms between H_2 and $\text{PuO}_2(111)$ surfaces, namely, stoichiometric/ideal $\text{PuO}_2(111)$ and reduced/defective $\text{PuO}_2(111)$ surfaces (see Fig. 1).

First of all, the effects of vdW forces upon H_2 molecule from the ideal- $\text{PuO}_2(111)$ surface are probed by an overall comparison between vdW-DFT+ U and DFT+ U calculated PEPs. We find that the pure DFT+ U calculations usually can not capture the physisorption state of

H_2 (with the adsorption energy E_{ad} of H_2 underestimated to less than 15 meV); not but what the vdW-DFT+ U scheme is able to do that. The improved description of H_2 physisorption by vdW-DFT+ U is particularly so when diatomic molecule H_2 is perpendicular to the ideal- $\text{PuO}_2(111)$ surface, for example, the F1- Z PEPs presented in Fig. 2(a). When H_2 drops from F1- Z of $h_0 = 4.5 \text{ \AA}$, the DFT+ U PEP indicates nearly an onefold force of repulsion existing between H_2 molecule and ideal- $\text{PuO}_2(111)$ surface, since the variation of relative energy as a function of h can be well fitted by $1/h$. However, the vdW-DFT+ U PEP shows the twofold interaction of both repulsion and attraction between H_2 and ideal- $\text{PuO}_2(111)$ surface, and thus the physisorption state of H_2 ($h \approx 2.2 \text{ \AA}$ and $E_{\text{ad}} \approx -0.10 \text{ eV}$) is well discerned mainly due to the vdW attractive force upon the H_2 from the ‘Tasker-type-II’ $\text{PuO}_2(111)$ surface, which is not entirely considered in the pure DFT+ U method. We note that the DFT+ U calculated E_{ad} of H_2 with the T1- Z geometry on the ideal- $\text{CeO}_2(111)$ surface is only ~ 20 meV [40], which is also notably underestimated. Since the surface O-vacancy can enhance the chemical activity of the inert ideal- $\text{PuO}_2(111)$ surface by efficiently lowering the surface work function [31], some DFT+ U PEPs seem to be able to give the weak physisorption states of H_2 on reduced- $\text{PuO}_2(111)$ with E_{ad} of only -50 meV more or less, but even so they can not really describe the interaction between H_2 and reduced- $\text{PuO}_2(111)$ because of the missing vdW force in the treatment. Figure 2(b) shows as an example the T2- Z PEP at reduced- $\text{PuO}_2(111)$. As a matter of fact, the surface O-vacancy will induce the local polarization of ideal- $\text{PuO}_2(111)$ surface and produce a stronger vdW attraction for H_2 . We can see from Fig. 2(b) that the vdW-DFT+ U calculated physisorption energy E_{ad} of H_2 near the O-vacancy (namely, $h \approx 1.3 \text{ \AA}$ over T2- Z site) on reduced $\text{PuO}_2(111)$ surface is about -0.17 eV instead of -50 meV from pure DFT+ U , and is somewhat higher of ~ 70 meV than the cases of H_2 on ideal- $\text{PuO}_2(111)$ such as F1- Z in Fig. 2(a). Therefore, in order to reasonably describe the multiple interaction between H_2 and Pu-oxide surfaces, we choose the vdW-DFT+ U scheme instead of pure DFT+ U method in the following static PEP calculations and AIMD simulations.

Figure 3(a)-(d) present all the vdW-DFT+ U PEPs of H_2 approaching the ideal- $\text{PuO}_2(111)$ surface considered in this work. One can see that H_2 molecules first undergo a weak physisorption state with $E_{\text{ad}} \geq -0.10 \text{ eV}$ when $h \geq 2.0 \text{ \AA}$, and then it seems to be hard for H_2 to get further close ($h \leq 2.0 \text{ \AA}$) to the inert surface, as the dominant force of repulsion between H_2 and ideal- $\text{PuO}_2(111)$ increases rapidly and notably raises the total

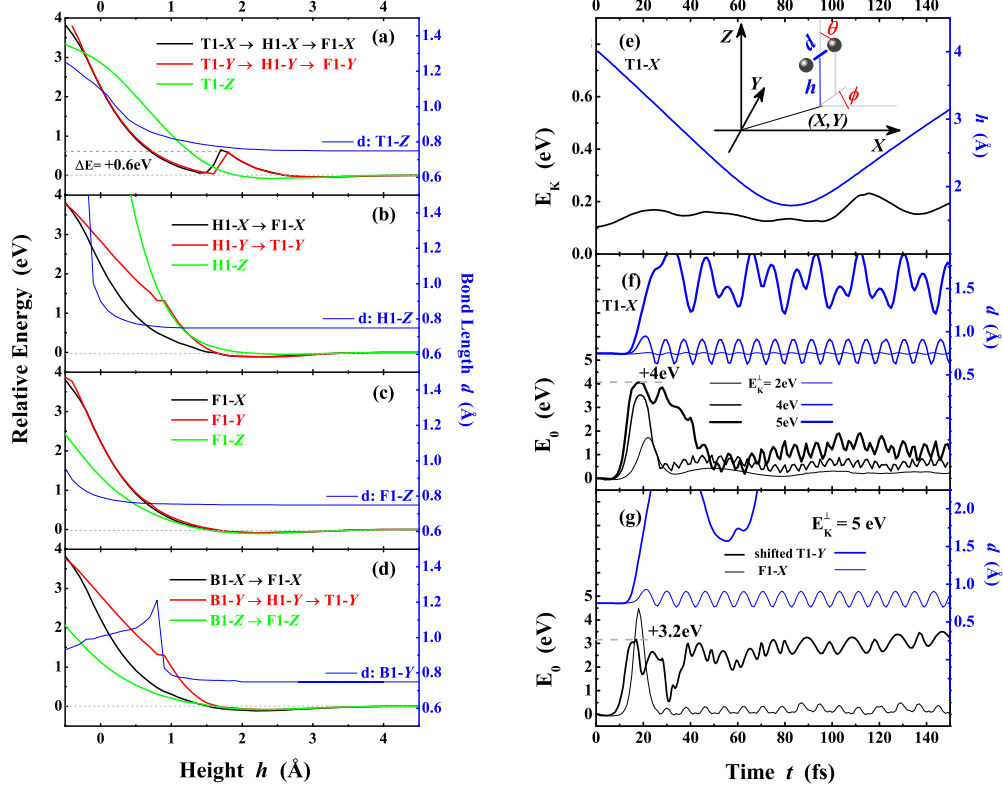


FIG. 3: (Color online) Left column: Static PEPs and bond-length d (in Å) of a H₂ molecule approaching the four different sites [namely, (a) T1, (b) H1, (c) F1, and (d) B1] on ideal-PuO₂(111) surface from different initial geometries, and the approximate directions of H₂ lateral migrations are indicated by arrows. Right column: AIMD results of the interaction dynamics for a H₂ impingement against ideal-PuO₂(111) surface. The inset shows the six degrees of freedom for H₂ on surface. When started from T1-X, the evolutions of (e) kinetic energy E_k (in eV) of the system and height h (in Å) of the H₂ molecule with initial E_k^\perp of 0.1 eV and (f) electronic free-energy E_0 of the system and d of H₂ for the increasing E_k^\perp . (g) Two limiting cases for the collision induced dissociation of H₂ with E_k^\perp of 5 eV, namely, started from shifted T1-Y and F1-X geometries.

energy of these systems, especially when $h \leq 1.0\text{ Å}$. We also find that many H₂ molecules can diverge away from their initial pathways driven by the lateral components of the repulsive force. These surface migrations of H₂ are labeled by their approximate directions in Figs. 3(a), 3(b), and 3(d). Much to our surprise, in Fig. 3(a) H₂ molecules with the T1-X and T1-Y initial geometries can first overcome an energy barrier of $\sim 0.6\text{ eV}$ at $h \approx 1.7\text{ Å}$ to migrate to H1 site, and then move towards F1 site. Among all these PEPs with h ranging from 4.5

to -0.5 \AA , none but the H1-Z PEP presents the dissociative adsorption of H_2 molecule when $h \leq -0.1 \text{ \AA}$ [see Fig. 3(b)], with one H atom binding to the subsurface Pu-cation and the other leaving over the surface, and the corresponding energy barrier is much higher than 4.0 eV, which indicates that the dissociative adsorption of H_2 on ideal- $\text{PuO}_2(111)$ surface should be an extremely endothermic and rare event. However, after artificially breaking the H-H bond, the adsorption energy E_{ad} of H atoms binding to the surface O anions is calculated to be -2.3 eV , which is really a very exothermic reaction to hydroxylate the $\text{PuO}_2(111)$ surface with H atoms. So that the dissociative adsorption should be the most stable and favorable state of H_2 molecule on ideal- $\text{PuO}_2(111)$ surface, which is also found to be similar to the strongly exothermic dissociation of H_2 on the ideal- $\text{CeO}_2(111)$ surface [39–41] with the E_{ad} of H atoms calculated by the DFT+ U to be about -2.6 eV . And the two OH groups formed on the oxide surface can help to reduce the nearby $\text{Pu}^{4+}/\text{Ce}^{4+}$ cations to +3 state.

Given the existing high barrier, the most controversial issue about the dissociative adsorption of H_2 actually rests with the reliable method to effectively simulate this extremely rare event and reasonably estimate the corresponding dissociation barriers. Recently, Alam *et al.* [42] have simulated the interaction process of hot H_2 molecule with the ideal- $\text{CeO}_2(111)$ and (110) surfaces by using the ultra accelerated quantum chemical molecular dynamic (UA-QCMD) method, which is based on the tight-binding quantum chemistry and the classical MD programs. In their UA-QCMD simulations, the mean velocity of several km/s was given to the H_2 molecule. Here, we perform comprehensive NVE-AIMD simulations to fulfil this task. From Fig. 3(e) we can see that if its initial kinetic energy is set at 0.1 eV, the initially nonrotating and nonvibrating H_2 from T1- X of $h_0 = 4.0 \text{ \AA}$ will bounce back to the vacuum soon and even can not touch the ideal- $\text{PuO}_2(111)$ surface. When the initial E_{k}^{\perp} of H_2 is less than 1.0 eV, the diffraction behaviors of molecular H_2 seem to be similar to the case presented in Fig. 3(e) without reference to its initial geometries. By continually elevating the initial E_{k}^{\perp} of H_2 up to 5.0 eV, we find that most of H_2 molecules parallelly hitting the ideal- $\text{PuO}_2(111)$ surface can be broken into two hot H atoms owning high velocities, which are expected to be captured by the surface O anions and eventually form two surface hydroxyl groups, i.e., the above-mentioned stable dissociative adsorption state of H_2 . Whereas, among all AIMD trajectories, the E_{k}^{\perp} -dependent dissociation behavior of H_2 from T1- X is an interesting exception and is thus presented in Fig. 3(f). It shows in Fig. 3(f) that (i) when the initial $E_{\text{k}}^{\perp} = 2.0 \text{ eV}$, H_2 can not touch the surface O-anion and bounce straightly

without arousing the molecular zero-point vibration, according to the inset of Fig. 7(b); (ii) when its E_k^\perp reaches 4.0 eV, the internal vibrational excitation of H_2 molecule emerges [$n = 1$ in Eq. (3)] after the head-on collision with the O-anion; (iii) until E_k^\perp reaches 5.0 eV, molecular H_2 is dissociated by its violent collision with surface O-anion. However, the products are not two hot H atoms but a hot H_2O molecule released to the vacuum and an O-vacancy left on the surface. This surface reduction process has also been reported by the above-mentioned UA-QCMD simulations of high-energy colliding H_2 molecule on $CeO_2(111)$ and (110) surfaces [42]. The energy barrier of collision induced dissociation process in this study is estimated to be ~ 4.0 eV based on the electronic free energy E_0 of this system in Fig. 3(f), which is close to the bond energy (~ 4.5 eV) of a free-standing H_2 molecule and indicates that the inert ideal- $PuO_2(111)$ surface can not act as the catalyst for H_2 dissociation. Since moisture can strongly enhance the further oxidation of Pu metal [5, 6], one can see that both the surface hydroxylation of PuO_2 by H_2 and the interaction between H_2O and PuO_2 surface are important topics, which will be investigated in our next work. In order to search out the possible lowest dissociation barrier, different incident conditions (namely, the initial E_k^\perp and the angles of incidence in some trajectories) are considered. Figure 3(g) presents two limiting cases. When E_k^\perp is 5.0 eV, the AIMD trajectory of H_2 started from the horizontally shifted T1- Y geometry (with one H-atom right above the surface O-anion) turns out to be the most possible dissociative adsorption path with the lowest barrier of ~ 3.2 eV. However, the trajectory started from F1- X indicates that H_2 will never dissociate even if we would further elevate the E_k^\perp in the NVE-AIMD simulation. Thus, the collision-dissociation behavior of H_2 is very site specific on ideal- $PuO_2(111)$ surface and depends heavily on the incident condition of H_2 . Overall, all the AIMD results well support the static PEPs and leads to a conclusion that the ideal- $PuO_2(111)$ surface is really difficult of access for H_2 molecule.

As the format of Fig. 3, Fig. 4 presents the interaction behaviors of H_2 molecule with the reduced- $PuO_2(111)$ surface, based on all static PEP results and some representative AIMD trajectories plotted in the left- and right-hand columns, respectively. From the vdW-DFT+ U PEPs, we can see that the molecular physisorption states are ubiquitous for H_2 on reduced- $PuO_2(111)$ surface when $h \geq 1.3 \text{ \AA}$, and the physisorption states of H_2 over the surface O-vacancy (i.e., T2 site) seem to be more stable than others, so that when further depressing the nearby adsorbed H_2 molecules, most of them tend to stride over certain

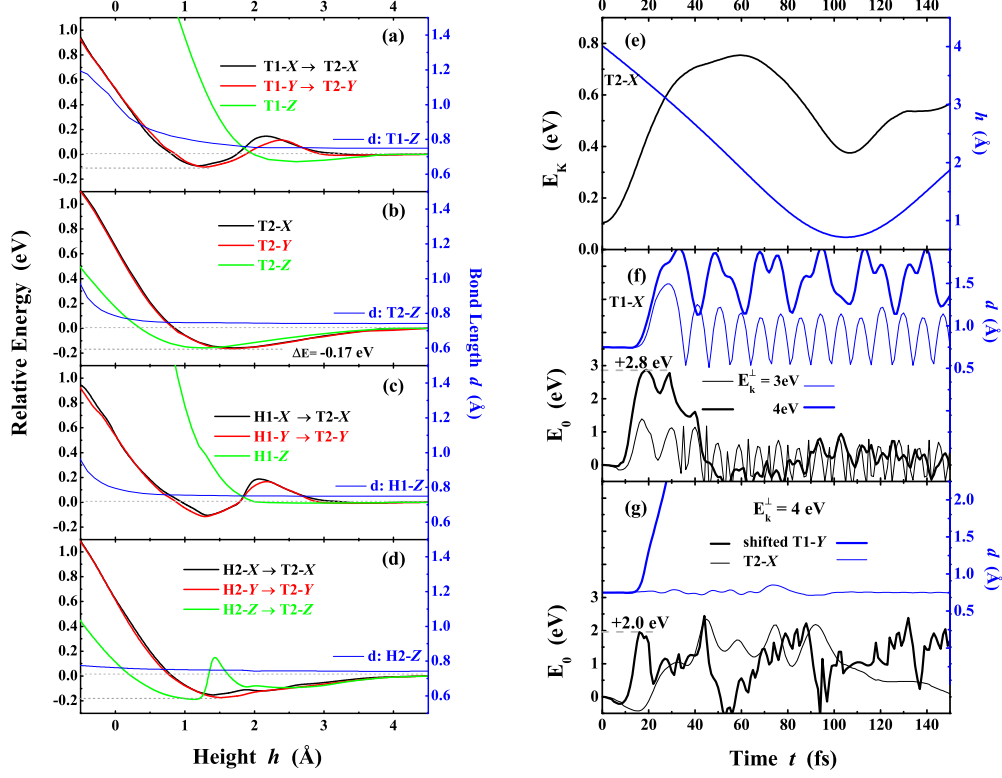


FIG. 4: (Color online) Left column: Static PEPs and d of a H₂ molecule approaching the four target sites [namely, (a) T1, (b) T2, (c) H1, and (d) H2] on reduced-PuO₂(111) surface from different initial geometries. Right column: AIMD results of H₂ interaction with reduced-PuO₂(111) surface. (e) Evolutions of E_k of the system and h of the H₂ molecule with initial geometry of T2-X and E_k^\perp of 0.1 eV. (f) Evolutions of E_0 of the system and d of the H₂ molecule started from T1-X with increasing E_k^\perp . (g) Two limiting cases for the collision induced dissociation of H₂ with E_k^\perp of 4 eV, i.e., started from shifted T1-Y and T2-X geometries.

barriers (less than 0.3 eV) to migrate to T2 site. Note that H₂ seems to get much closer to the reduced-PuO₂(111) surface than to the ideal-PuO₂(111) surface mainly because of the 25% O-vacancy on the former. However, when $h \leq 1.3$ Å, it becomes more and more difficult for H₂ to get further closer to the surface and all these PEPs with h ranging from 4.5 to -0.5 Å do not present the dissociative adsorption of H₂, which is to some extent similar to the behavior of H₂ on ideal-PuO₂(111) surface.

Figure 4(e) shows the total kinetic energy E_k of the system and the bond-length d of H₂ with its initial E_k^\perp of 0.1 eV along AIMD trajectory started from T2-X of $h_0 = 4.0$ Å. We can

see that during the initial 60 fs, the vdW force of attraction causes the steady augmentation of E_k , and then the increasing force of repulsion exceeds the vdW force and pushes H_2 back to the vacuum. Meanwhile, the zero-point vibration of H_2 is aroused. Comparing Fig. 3(e) with Fig. 4(e), we can see that the interaction of H_2 with ideal- and reduced-PuO₂(111) surfaces are actually unlike, and the surface O-vacancy modulates the interaction behavior between H_2 and PuO₂(111) surfaces by changing the surface atomic and electronic structure properties. Based on enough NVE-AIMD trajectories of H_2 impinging against the reduced-PuO₂(111) surface, we also try to reveal the possible dissociation behavior and search out the lowest dissociation barrier of H_2 on reduced-PuO₂(111) surface. We find that several contact collisions between H_2 and reduced-PuO₂(111) can not occur until the initial E_k^\perp of H_2 reaches 1.0 eV, which is consistent with most of the PEPs in the left-hand column of Fig. 4. When the E_k^\perp of H_2 reaches 4.0 eV, the collision induced dissociation of H_2 will take place to yield two hot H atoms in most AIMD trajectories. Whereas, the trajectory started from T1- X still make an interesting exception, which is revealed in Fig. 4(f). From Fig. 4(f), we can see that when $E_k^\perp = 3.0$ eV, after the quick migration [from T1 to T2 site driven by the repulsive force, see Fig. 4(a)] and the subsequent collision (at T2 site), the rebounded H_2 molecule seems to be at the second vibrational excitation state [$n = 2$ in Eq. (3)]. When E_k^\perp reaches 4.0 eV, without the lateral migration, the H_2 molecule straight hits the O-anion target to break its bond, and soon two hot H atoms pull the O-anion out of the surface to yield a hot H_2O molecule released to the vacuum. Upon that, when starting from T1- X , the collision-dissociation dynamics of H_2 on reduced-PuO₂(111) surface is similar to that occurred on the ideal-PuO₂(111) surface. However, the corresponding dissociation barriers are quite different, namely, 2.8 and 4.0 eV for H_2 on reduced- and ideal-PuO₂(111) surfaces, respectively. For the dissociation possibility of H_2 (with $E_k^\perp = 4.0$ eV) on reduced-PuO₂(111) surface, Fig. 4(g) presents two limiting cases as follows: (i) The AIMD trajectory started from the horizontally shifted T1- Y geometry [as in Fig. 3(g)] gives the lowest energy barrier of ~ 2.0 eV, much lower than the lowest barrier ~ 3.2 eV in Fig. 3(g); (ii) Whereas, the trajectory started from T2- X (or T2- Y , not shown here) indicates that H_2 will never dissociate even with a higher E_k^\perp . Given the incidental migrations of H_2 from other sites to T2 (see the PEP results in Fig. 4), we can conclude that the reduced-PuO₂(111) surface is also difficult of access for H_2 molecule, let along the collision induced dissociation.

If H_2 is barely able to react with PuO₂(111) surfaces, as the smallest diatomic molecule,

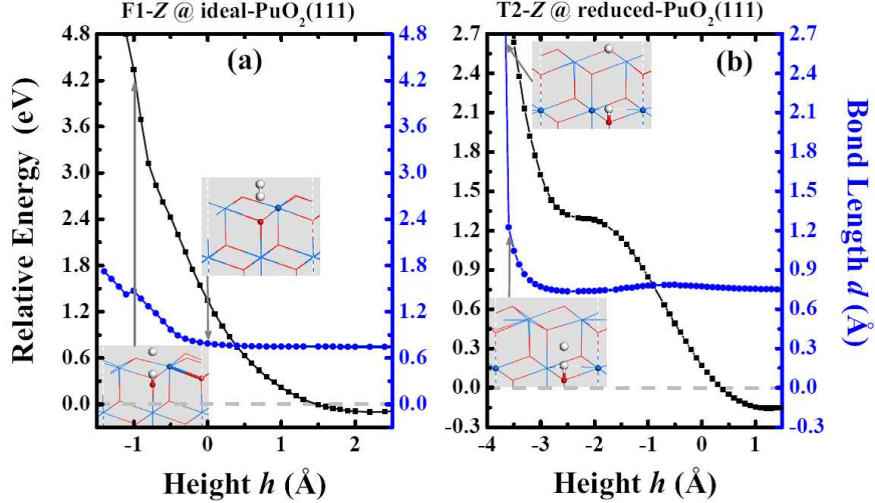


FIG. 5: (Color online) Calculated PEPs and d of a H_2 penetration into (a) the ideal- $\text{PuO}_2(111)$ surface from the F1- Z physisorption state; and (b) the reduced- $\text{PuO}_2(111)$ from T2- Z . The total energies of starting geometries with $h_0 = 4.5 \text{ \AA}$ are set to 0 eV and four insets show the atomic structures of the corresponding reference points.

is there any possibility for it to penetrate vertically into the $\text{PuO}_2(111)$ overlayers? As the continuations of the vdW-DFT+ U PEPs in Fig. 2(a) and 2(b), the PEPs for H_2 penetration into ideal- and reduced- $\text{PuO}_2(111)$ surfaces from the corresponding physisorption states are presented in Fig. 5(a) and 5(b), respectively. We can see from Fig. 5(a) that the relative energy of the system increases fleetly during the penetration of H_2 molecule into ideal- $\text{PuO}_2(111)$ surface, wherein two insets show atomic structures of two reference points (namely, $h = 0$ and -1.0 \AA). Since H_2 touches the surface ($h = 0 \text{ \AA}$), its bond ($d = 0.8 \text{ \AA}$) is stretched notably, and once the whole H_2 enters the surface ($h = -1.0 \text{ \AA}$), the H-H bond is snapped ($d = 1.5 \text{ \AA}$) with one H atom binding to the subsurface Pu-cation and the other segregating out of the surface. Upon that, the penetration of H_2 molecule into ideal- $\text{PuO}_2(111)$ surface is too endothermic to occur under ambient conditions because the stoichiometric PuO_2 is so close-grained that the H_2 needs to overcome a high energy barrier of more than 4 eV to be broken before squashing in the PuO_2 overlayer. For the penetration of H_2 molecule into reduced- $\text{PuO}_2(111)$ surface, we can see from Fig. 5(b) that the PEP curve of T2- Z is stepwise, namely, the relative energy first increases rapidly during molecular entry into the surface ($-1.5 \leq h \leq 1.3 \text{ \AA}$) with the penetration barrier of $\sim 1.5 \text{ eV}$, then

increases slowly for the subsurface migration of H_2 ($-3.0 \leq h \leq -1.5 \text{ \AA}$), and ultimately increases sharply when H_2 approaches and binds to the Pu-cation. Once the H_2 reacts with the Pu-cation below, it will dissociate (see the lower inset), and soon the upper H-atom will be segregated out and stay at the site of surface O-vacancy binding with three Pu cations nearby (see the upper inset). Before molecular dissociation, interestingly, the H-H bond is first stretched slightly while H_2 is hauled step by step into the surface, and then relaxes back to the equilibrium state after H_2 entry into the surface, which differs from the variation of d in Fig. 5(a) and indicates that just one surface O-vacancy can let the smallest H_2 molecule enter the PuO_2 surface layer. But the further penetration of H_2 in PuO_2 overlayer ($h \leq -3.0 \text{ \AA}$) is found to be very difficult since H_2 meets with the close-grained $\text{PuO}_2(111)$ subsurface layer subsequently.

Thus, according to our current comprehensive study of the interaction properties between H_2 molecule and $\text{PuO}_2(111)$ surfaces, it is found that the close-grained PuO_2 overlayer can efficiently prevent the penetration and diffusion of hydrogen (into the Pu-oxide film), and protect the underlying Pu-metal from hydrogenation.

B. The interaction between H_2 and $\alpha\text{-Pu}_2\text{O}_3(111)$ surface

In this subsection, we turn to study the interaction mechanisms between H_2 and the stoichiometric $\alpha\text{-PuO}_2(111)$ surface. Note that in addition to the formation of 25% oxygen vacancies, there is an interesting volume expansion (7.6% in theory and 7.4% in experiment) during the $\text{PuO}_2 \rightarrow \text{Pu}_2\text{O}_3$ isostructure reduction mainly due to the strong on-site Coulomb repulsion among the Pu-5*f* electrons [32]. Thus, compared to the close-grained and smooth $\text{PuO}_2(111)$ surface, the $\alpha\text{-Pu}_2\text{O}_3(111)$ seems to be a porous slab with 25% native O vacancies located on every O-layer, and its surface is not smooth any more.

Four representative PEPs of H_2 molecule approaching $\alpha\text{-Pu}_2\text{O}_3(111)$ surface are shown in Fig. 6(a). One can see that when H_2 molecule is dropped from T1-*X* and F2-*X* geometries, the corresponding PEPs are similar to those PEPs of H_2 approaching ideal- $\text{PuO}_2(111)$ surface [see Figs. 3(a)-(d)], and thus the T1 and F2 sites on $\alpha\text{-Pu}_2\text{O}_3(111)$ surface are also very difficult of access. However, when starting from T3-*X* or T3-*Z*, after the weak physisorption states, H_2 molecule can further be pulled into the $\alpha\text{-Pu}_2\text{O}_3(111)$ overlayer via the surface O-vacancy, which is similar to the case of H_2 entry into the reduced- $\text{PuO}_2(111)$ surface [see

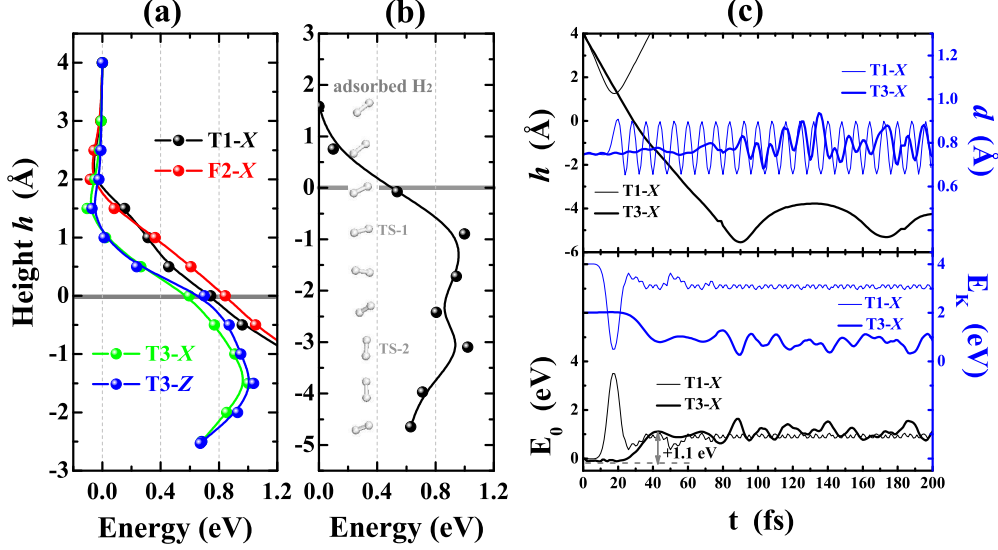


FIG. 6: (Color online) (a) Calculated PEPs for H₂ interaction with α -Pu₂O₃(111) surface. (b) Calculated MEP for H₂ penetration from the physisorption state at T2, with the orientations of H₂ during penetration shown by the inset. (c) AIMD results of H₂ interaction with α -Pu₂O₃(111): h and d of H₂ (upper panel) and E_0 and E_K of system (lower panel) for H₂ dropped from T1-X (with $E_k^\perp = 4.0$ eV) and T3-X (with $E_k^\perp = 2.0$ eV) geometries.

Fig. 5(b)]. The energy barrier of H₂ molecule penetration into α -Pu₂O₃ reported by the PEPs is ~ 1.1 eV less than the barrier of ~ 1.5 eV for H₂ entry the reduced-PuO₂(111). In order to accurately obtain the energy barrier and the rate constant $k_{\text{hTST}}^{\text{Pen}}$ of H₂ penetration, we first use the CI-NEB method [55] with seven images to search out the transition-state (TS) from the minimum energy pathway (MEP), and then calculate the vibrational frequencies of H₂ molecule at the initial physisorption-state (IS) and the TS. The MEP result and the orientations of H₂ molecule during the penetration process are plotted in Fig. 6(b). One can see that there are two TSs for H₂ molecule first entry (TS-1) and then diffusion (TS-2) in the α -Pu₂O₃ overlayer, respectively. And H₂ at TS-1 almost horizontally locates ~ 1.0 Å below the surface-layer (with the penetration barrier of ~ 1.0 eV) but H₂ at TS-2 tends to be perpendicular to the surface (with the diffusion barrier of ~ 0.21 eV), indicating that H₂ seems to be able to rotate freely in the tunnel made of the vertically distributed O vacancies.

Based on the vibrational frequencies of H₂ listed in Table I, we can see that H₂ at the IS vibrates, nearly like a free molecule, with mainly a symmetric stretching vibration

TABLE I: Calculated normal vibration frequencies ν_n (in THz, n=1-6) of H₂ molecule with the IS, the TS-1 and the TS-2 structures.

	ν_1	ν_2	ν_3	ν_4	ν_5	ν_6
IS	129.43	9.21	7.36	3.85	1.26	0.84
TS-1	120.64	31.34	18.14	10.85	3.82	9.14(i)
TS-2	122.09	21.46	21.32	11.81	11.04	7.46(i)

($\nu_1 = 129.43$ THz). Whereas, H₂ at both TSs vibrates somewhat complicatedly under the influence of α -Pu₂O₃ matrix and has one imaginary frequency. At the room temperature of $T = 300$ K, the $k_{\text{hTST}}^{\text{Pen}}$ of H₂ is estimated to be $\sim 2 \times 10^{-7}$ /s, which is really small mainly due to the relatively high penetration barrier (1.0 eV) of H₂ entry the stoichiometric α -Pu₂O₃(111) overlayer. However, in practice the Pu-oxide overlayer on Pu-metal is really far from being an ideal (defect-free) PuO₂ or Pu₂O₃, and other defects such as microcracks or some forms of impurity inclusions in the overlayer can prominently promote the probability of H₂ penetration. Therefore, it is certainly one challenging task to predict and control the length of induction period in Pu-hydrogenation. Here, at the atomic and molecular level, we just focus on understanding the different roles of ideal PuO₂ and α -Pu₂O₃ overlayers in Pu-hydrogenation, and at this point our theoretical results have well revealed the major difference between PuO₂ and α -Pu₂O₃, namely, PuO₂ is airtight but α -Pu₂O₃ is porous for the smallest H₂ molecule.

Furthermore, the AIMD simulations are also performed to depict the interaction dynamics for H₂ impingement against the α -PuO₂(111) surface. Figure 6(c) shows the representative NVE-AIMD trajectories started from the T1-*X* and T3-*X* with $h_0 = 4$ Å, where the evolutions of height h and bond-length d of H₂ (upper panel), the relative electronic free-energy E_0 , and the kinetic energy E_k of the system (lower panel) are shown. We can see that even when the initial E_k^\perp reaches 4.0 eV, H₂ seems to be unable to touch the T1 site on α -Pu₂O₃(111) surface ($h \geq 1.2$ Å) and soon bounces back with the zero-point vibration, which is very unlike the dissociation of H₂ (with E_k^\perp of 4.0 eV) on reduced-PuO₂(111) surface [see Fig. 4(f)] but is like the diffraction behavior on ideal-PuO₂(111) surface [see Fig. 3(f)]. The reasons are that (i) the α -Pu₂O₃(111) surface is not smooth with many protrusions such as the T1 site, and actually H₂ can contact the O-anion at T1 site; and (ii) on the other hand

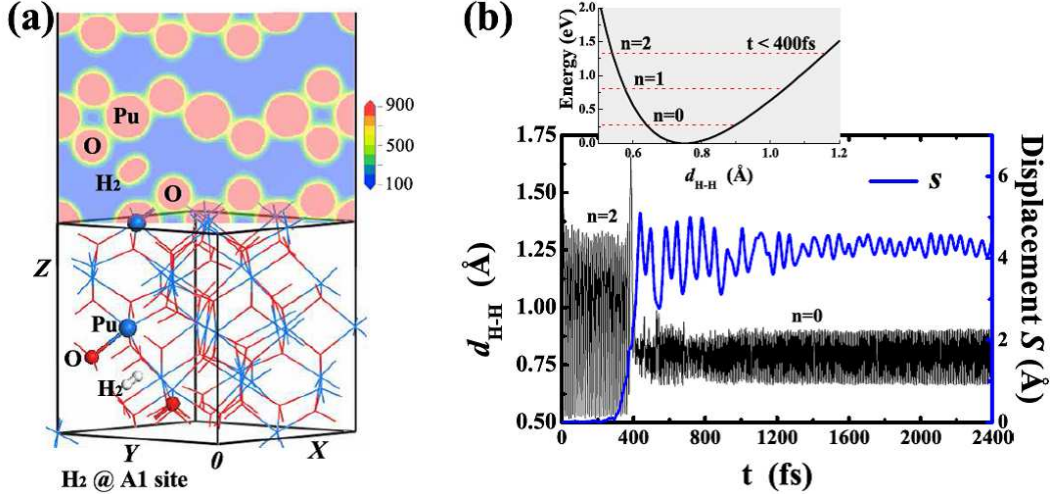


FIG. 7: (Color online) (a) Section plane of total electron-density (top) and atomic structure (bottom) of α -Pu₂O₃ matrix with a H₂ molecule at A₁ site. (b) NVE-AIMD evolutions of d and displacement s of a H₂ molecule with internal vibrational excitation ($n = 2$ as shown by the inset) in α -Pu₂O₃.

it will take much more energy to dig an O-anion out of the surface since further reduction of α -Pu₂O₃ is very difficult [32]. However, the H₂ molecule with an initial E_{k}^{\perp} of 2.0 eV can stride over an energy barrier of ~ 1.1 eV to penetrate via T3 site into the α -Pu₂O₃(111) overlayer, and then diffuses easily along the devious alleyway made of the continuous distributed O vacancies. During the H₂ penetration and diffusion, the internal vibration of H₂ molecule is fitful and is especially so after the first collision with Pu-cation ($t = 90$ fs). Although the inhalation of a H₂ molecule in the α -Pu₂O₃(111) slab is endothermic (see E_0 of the system), the hot H₂ molecule can release the redundant kinetic energy and change the direction of movement via successive collisions with α -Pu₂O₃ matrix, and as a result H₂ seems to be neither escape out of nor dissociate in α -Pu₂O₃(111) during the simulation process of 3 ps.

In order to gain detailed insights into the adsorption states and the diffusion behaviors of H₂ molecule in the α -Pu₂O₃(111) matrix, we first carry out systematic total-energy calculations to search for favorable sites for H₂ to stay at. Then, based on the AIMD simulations within canonical ensemble (NVT-AIMD), we discuss the temperature effect on the state or behavior of H₂ in α -Pu₂O₃. Figure 8(a) shows four relatively favorable molecular mass-center sites A_{*n*} ($n=1-4$) for H₂ adsorption, and the adsorption energies of H₂ at these four sites are

TABLE II: Calculated bond-length d (in Å), adsorption energy E_{ad} (in eV), and stretching vibration frequencies ν_1 (in THz) of H_2 molecule at four adsorption states A_n and four transition states T_n ($n=1-4$). Calculated room-temperature (300 K) rate constant $k_{\text{hTST}}^{\text{Diff}}$ (in s^{-1}) of the bilateral diffusion of H_2 in $\alpha\text{-Pu}_2\text{O}_3$ is also listed.

	A_1	T_1	A_2	T_2	A_3	T_3	A_4	T_4
d	0.760	0.751	0.760	0.764	0.765	0.758	0.767	0.765
E_{ad}	0.665	0.925	0.669	1.125	0.606	0.845	0.601	1.134
ν_1	120.84	124.27	120.70	118.38	118.88	121.30	118.21	116.84
$k_{\text{hTST}}^{\text{Diff}}$	\rightarrow	1.75×10^9	\rightarrow	2.81×10^4	\rightarrow	5.16×10^9	\rightarrow	7.22×10^3
$k_{\text{hTST}}^{\text{Diff}}$	\leftarrow	2.18×10^9	\leftarrow	4.94×10^3	\leftarrow	3.21×10^9	\leftarrow	1.90×10^4

listed in Table II, where H_2 molecule can rotate slightly around the four sites and the A_4 site seems to be a little more favorable with a positive (endothermic) adsorption energy E_{ad} of +0.601 eV. Subsequent NVT-AIMD simulations at three temperatures ($T = 300, 600,$ and 900 K) show that the molecules just move around their initial adsorption sites with the zero-point vibration and do not diffuse or dissociate within the isothermal period of 5 ps. The atomic adsorption energy is calculated to be endothermic (+0.69 eV/atom), which indicates that the dissociative adsorption of H_2 in $\alpha\text{-Pu}_2\text{O}_3$ should be more endothermic than the molecular adsorption. Thus, in contrary to the slightly exothermic adsorption of H atom to form OH group in bulk PuO_2 , H_2 molecule and even H atom can not easily react with the $\alpha\text{-Pu}_2\text{O}_3$ matrix since the reduction of $\alpha\text{-Pu}_2\text{O}_3$ is much more difficult than that of PuO_2 [32]. The exothermic adsorption of H atom in bulk PuO_2 is also found to be similar to that of H atom in CeO_2 [56], which can reduce the +4 cation in both fluorite-structured oxides.

According to Table II, the adsorption properties of H_2 molecules at four sites seem to be close to each other, and their temperature-dependent behaviors in $\alpha\text{-Pu}_2\text{O}_3$ are also very similar. For the convenience of depiction, we just plot in Fig. 7(a) the atomic- and electronic-structure results of the A_1 -site adsorption system. We can see that the H_2 molecule actually stays in suspension at A_1 site, which is near the location of an O-anion in the isostructure PuO_2 supercell, i.e., the native O-vacancy site in $\alpha\text{-Pu}_2\text{O}_3$. The charge density distribution in Fig. 7(a) indicates that there is no evidence of chemical binding of H_2 molecule to the

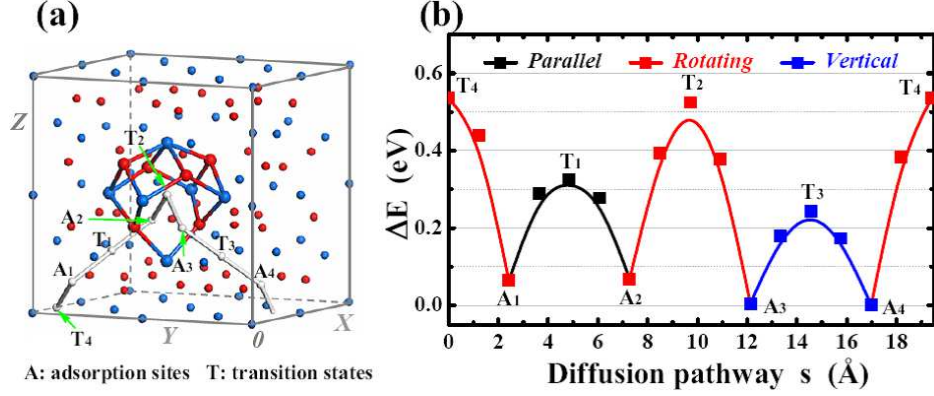


FIG. 8: (Color online) (a) Four adsorption sites A_1 - A_4 and four transition-state sites T_1 - T_4 of H_2 in α - Pu_2O_3 , which are linked with thick white lines to indicate the whole diffusion path of H_2 . (b) MEPs between adjacent adsorption sites, with the A_4 -site adsorption state as the reference point ($E_0 = 0$ eV). Lines of different colors are used to guide the eyes.

nearby Pu-cation or O-anion, and there seems to be enough space for the movement or diffusion of H_2 molecule in the α - Pu_2O_3 matrix. Furthermore, in the NVE-AIMD, we first consider the internal vibrational excitation of H_2 molecule at A_1 site [with $n = 2$ in Eq. (3)] and then let the system relax freely, as is shown in Fig. 7(b). We find that during the initial 400 fs, the H_2 vibrates drastically at A_1 site. Then, this hot H_2 molecule touches the nearby Pu-cation at $t = 400$ fs, and meanwhile transforms most of the vibration energy into the translation and rotation energy. Soon after that, H_2 migrates quickly to the A_2 site and transfers its kinetic energy towards the vibration of the α - Pu_2O_3 matrix via the successive collisions with the matrix within ~ 400 fs. Eventually ($t \geq 800$ fs), the H_2 molecule at A_2 site comes back to the zero-point vibration state after releasing most of its kinetic energy. The displacement S of H_2 as a function time ($t \leq 2.4$ ps) plotted in Fig. 7(b) indicates that the local movement ($A_1 \rightarrow A_2$) of H_2 is easy but the long-distance diffusion through the four sites seems to be very time-consuming, which can not be directly studied by the AIMD simulations. Overall, this interesting example reveals that the H_2 molecule tends to keep its ground state with the zero-point vibration.

Figure 8(a) shows that the four sites in a crystal cell of α - Pu_2O_3 are actually connectible by the O-vacancy distributed continuously in the α - Pu_2O_3 matrix, so that if given enough time, H_2 can penetrate through the α - Pu_2O_3 overlayer and the diffusion of H_2 in α - Pu_2O_3

seems to be continuous in a stepwise way. By using the CI-NEB method, we search out four TSs [with their sites labeled by T_n ($n=1-4$) in Fig. 8(a)] from the calculated minimum energy pathways (MEPs) between adjacent sites, which are plotted in Fig. 8(b). We can see from Fig. 8 that (i) the whole diffusion pathway is a close loop and consists of four short routes in the periodical α -Pu₂O₃ matrix; and (ii) when diffusing along the linear routes (from A₁ to A₂ and from A₃ to A₄, and vice versa), the H₂ can keep parallel and vertical to the routes and the corresponding lowest diffusion barriers are 0.26 eV (A₁ → A₂) and 0.24 eV (A₃ → A₄); whereas (iii) when migrating along the meandering routes (A₄ ⇌ A₁ and A₂ ⇌ A₃). The corresponding rightward diffusion barriers are doubled to be 0.53 and 0.46 eV because H₂ needs to rotate during the migration courses and swerve at the transition states (T₂ and T₄). Furthermore, we calculate the vibrational frequencies of H₂ at four adsorption sites and four transition states, with the major stretching vibration frequencies listed in Table II. Then, following Eq. (4), we figure out the rate constant ($k_{\text{hTST}}^{\text{Diff}}$) of H₂ diffusion in bulk α -Pu₂O₃ and list the calculated results of $k_{\text{hTST}}^{\text{Diff}}$ at room temperature ($T = 300$ K) in Table II. We can see that the $k_{\text{hTST}}^{\text{Diff}}$ of H₂ diffusion from a metastable state to a relative stable state is always larger than the $k_{\text{hTST}}^{\text{Diff}}$ of the reverse diffusion, and the probabilities for H₂ diffusion along linear routes (A₁ ⇌ A₂ and A₃ ⇌ A₄) are about five or six orders of magnitude larger than the case of H₂ migration along meandering routes, indicating that the diffusion kinetics of H₂ in α -Pu₂O₃ is mainly determined by the thermodynamical parameter diffusion barrier.

Assuming sequential first-order kinetics, the overall diffusion rate for H₂ in the α -Pu₂O₃ crystal cell can be simply estimated as $\frac{1}{k_{\text{overall}}^{\text{Diff}}} = \sum_{i=1}^4 \frac{1}{k_i^{\text{Diff}}}$, where k_i^{Diff} is the rate constant of the i th step diffusion. At 300 K, the rightward (A₁ → A₄) $k_{\text{overall}}^{\text{Diff}}$ of H₂ in α -Pu₂O₃ is $\sim 5.7 \times 10^3$ /s, and the leftward one is $\sim 3.9 \times 10^3$ /s, indicating that the H₂ migration along meandering routes is the rate-determining step for the diffusion kinetics of H₂ in α -Pu₂O₃. Considering the small $k_{\text{hTST}}^{\text{Pen}}$ of $\sim 2 \times 10^{-7}$ /s for H₂ penetration into α -Pu₂O₃(111) overlayer, the diffusion of H₂ in bulk α -Pu₂O₃ seems to be much easier since the $k_{\text{overall}}^{\text{Diff}}$ is at least ten orders of magnitude larger than the $k_{\text{hTST}}^{\text{Pen}}$. Thus, under oxygen-poor conditions, the course of H₂ entry the α -Pu₂O₃ overlayer is the final rate-determining step for H₂ penetration through the α -Pu₂O₃ to reach the Pu-metal. In order to quantitatively determine the rate constants of H₂ penetration, the practical surface configuration of α -Pu₂O₃ overlayer is a critical factor. But the complex surface conditions of oxide-coated Pu are undoubtedly

not as simple as the stoichiometric α -Pu₂O₃(111) surface considered in this work, so that we just take the first step towards understanding the hydrogenation of Pu-oxide coated Pu metal.

IV. CONCLUSIONS

In summary, based on the vdW-DFT+ U scheme, we have explored the different roles of the Pu-oxide overlayers in the hydrogenation of Pu underlayer. Three model surfaces of Pu-oxides are considered by varying oxygen conditions. We have found that the physisorption state of H₂ on PuO₂(111) surfaces can not be captured by pure DFT+ U calculations until the van der Waals correction is taken into account. We have shown that the surface O-vacancy induces a local polarization and produce a stronger van der Waals attraction for H₂, thus the physisorption energy of H₂ near the O-vacancy on the reduced PuO₂(111) surface becomes higher by ~ 70 meV than that on the ideal PuO₂(111) surface. However, the physisorbed H₂ molecules can not further get close to PuO₂(111) surfaces. In agreement with the static PEP results, our AIMD simulations have shown that the H₂ molecule will bounce back to the vacuum when its initial kinetic energy is not high enough. Until the initial E_k^\perp reaches ~ 5.0 eV (~ 4.0 eV), the H₂ molecule parallel to stoichiometric (reduced) PuO₂(111) surface can be broken. Interestingly, these collision-induced dissociation behaviors of H₂ have been found to be very site-specific. For instance, two H atoms can chemically bind with two O-anions to form hydroxyl groups and can also react with one O-anion to produce a H₂O molecule. Although the dissociative adsorption of H₂ is very exothermic and can reduce PuO₂(111) surfaces, it should be an extremely rare event due to the high energy barriers (3.2 and 2.0 eV for H₂ on the ideal- and reduced-PuO₂(111) surfaces, respectively). Therefore, the close-grained PuO₂ overlayer acts as a diffusion barrier to control the permeation of hydrogen and lengthen the initiation time of Pu-hydrogenation.

As a product of isostructure reduction of PuO₂, α -Pu₂O₃ has 25% oxygen vacancies located along $\langle 111 \rangle$ diagonals and thus seems to be a porous slab. Our AIMD study have directly revealed that the H₂ molecule can overcome an barrier of ~ 1.0 eV and directly penetrate into the α -Pu₂O₃(111) film via the O vacancies. By examining the temperature effect and the internal vibrational excitations of H₂, we have also provided a detailed insight into the interaction dynamics between H₂ and α -Pu₂O₃. In α -Pu₂O₃, the hot H₂ molecule

prefers to release its energy via successive collisions and come back to its ground state with zero-point vibration. The diffusion behavior of H₂ in α -Pu₂O₃ is also systematically investigated by searching out the minimum diffusion paths and calculating the diffusion rate constants of H₂. Our results are consistent with the general experimental observations, and come to the conclusion that the PuO₂ overlayer can hinder the hydrogen penetration, provided the isostructure reduction of PuO₂ to α -Pu₂O₃ is efficiently suppressed.

Acknowledgments

This work was supported by the Foundations for Development of Science and Technology of China Academy of Engineering Physics under Grants Nos. 2010B0301048, 2011A0301016, and 909-07, and partially supported by the NSFC under Grants No. 11004012, No. 51071032, No. 11205019. and No. 11275032.

-
- [1] S. Y. Savrasov and G. Kotliar, Phys. Rev. Lett. **84**, 3670 (2000).
 - [2] L. Petit, A. Svane, Z. Szotek, W. M. Temmerman, Science **301**, 498 (2003).
 - [3] K. T. Moore and G. van der Laan, Rev. Mod. Phys. **81**, 235 (2009).
 - [4] J. X. Zhu, R. C. Albers, K. Haule, G. Kotliar and J. M. Wills, Nat. Commun. **4**, 2644 (2013).
 - [5] C. A. Colmenares, Prog. Solid St. Chem. **9**, 139 (1975).
 - [6] J. M. Haschke, Los Alamos Science **26**, 253 (2000).
 - [7] M. T. Butterfield, T. Durakiewicz, I. D. Prodan, G. E. Scuseria, E. Guziewicz, J. A. Sordo, K. N. Kudin, R. L. Martin, J. J. Joyce, A. J. Arko, K. S. Graham, D. P. Moore, and L. A. Morales, Surf. Sci. **600**, 1637 (2006).
 - [8] H. A. Wriedt, Bull. All. Ph. Dia. **11**(2), 184-202 (1990).
 - [9] M. T. Butterfield, T. Durakiewicz, E. Guziewicz, J. Joyce, A. Arko, K. Graham, D. Moore, and L. Morales, Surf. Sci. **571**, 74 (2004).
 - [10] J. M. Haschke, T. H. Allen, and L. A. Morales, Science **287**, 285 (2000).
 - [11] P. A. Korzhavyi, L. Vitos, D. A. Andersson and B. Johansson, Nature Mater. **3**, 225 (2004).
 - [12] T. Gouder, A. Seibert, L. Havela, and J. Rebizant, Surf. Sci. **601**, L77 (2007).
 - [13] H. G. García Flores, P. Roussel, D. P. Moore, D. L. Pugmire, Surf. Sci. **605**, 314 (2011).

- [14] P. Morrall, S. Tull, J. Glascott, P. Roussel, J. Alloys Comp. **444-445**, 352-355 (2007).
- [15] L. N. Dinh, J. M. Haschke, C. K. Saw, P. G. Allen, W. McLean II, J. Nucl. Mater. **408**, 171 (2011).
- [16] G. W. McGillivray, J. P. Knowles, I. M. Findlay, M. J. Dawes, J. Nucl. Mater. **412**, 35 (2011).
- [17] C. E. Boettger and A. K. Ray, Int. J. Quantum Chem. **90**, 1470 (2002).
- [18] C. McNeilly, J. Nucl. Mater. **11**, 53 (1964).
- [19] S. L. Dudarev, G. A. Botton, S. Y. Savrasov, C. J. Humphreys, and A. P. Sutton, Phys. Rev. B **57**, 1505 (1998).
- [20] L. Petit, A. Svane, Z. Szotek, W. M. Temmerman, and G. M. Stocks, Phys. Rev. B **81**, 045108 (2010).
- [21] I. D. Prodan, G. E. Scuseria, J. A. Sordo, K. N. Kudin, and R. L. Martin, J. Chem. Phys. **123**, 014703 (2005).
- [22] Q. Yin and S. Y. Savrasov, Phys. Rev. Lett. **100**, 225504 (2008).
- [23] B. Sun, P. Zhang, and X.-G. Zhao, J. Chem. Phys. **128**, 084705 (2008).
- [24] B. Sun, and P. Zhang, Chin. Phys. B **18**, 1364 (2008).
- [25] P. Zhang, B.-T. Wang, and X.-G. Zhao, Phys. Rev. B **82**, 144110 (2010).
- [26] G. Jomard, B. Amadon, F. Bottin, and M. Torrent, Phys. Rev. B **78**, 075125 (2008).
- [27] D. A. Andersson, J. Lezama, B. P. Uberuaga, C. Deo, and S. D. Conradson, Phys. Rev. B **79**, 024110 (2009).
- [28] H. Shi, M. Chu, and P. Zhang, J. Nucl. Mater. **400**, 151 (2010).
- [29] H. Shi, and P. Zhang, J. Nucl. Mater. **420**, 159 (2012).
- [30] G. Jomard, and F. Bottin, Phys. Rev. B **84**, 195469 (2011).
- [31] B. Sun, H. Liu, H. Song, G. Zhang, H. Zheng, X.-G. Zhao, and P. Zhang, J. Nucl. Mater. **426**, 139 (2012).
- [32] B. Sun, H. Liu, H. Song, G. Zhang, H. Zheng, X.-G. Zhao, and P. Zhang, Phys. Lett. A **376**, 2672 (2012).
- [33] B. McCart, G. H. Lander, and A. T. Aldred, J. Chem. Phys. **74**, 5263 (1981).
- [34] M. Wulff and G. H. Lander, J. Chem. Phys. **89**, 3295 (1988).
- [35] P. Santini, R. Lémanski, and P. Erdős, Adv. Phys. **48**, 537 (1999).
- [36] M. Colarieti-Tosti, O. Eriksson, L. Nordström, J. Wills, and M. S. S. Brooks, Phys. Rev. B **65**, 195102 (2002).

- [37] S. Kern, R. A. Robinson, H. Nakotte, G. H. Lander, B. Cort, P. Watson, and F. A. Vigil, *Phys. Rev. B* **59**, 104 (1999).
- [38] G. Raphael and R. Lallement, *Solid State Commun.* **6**, 383 (1968).
- [39] G. Vicario, G. Balducci, S. Fabris, S. Gironcoli, and S. Baroni, *J. Phys. Chem. B* **110**, 19380 (2006).
- [40] H.-T. Chen, Y. M. Choi, M. Liu, and M. C. Lin, *ChemPhysChem* **8**, 849 (2007).
- [41] M. B. Watkins, A. S. Foster, and A. L. Shluger, *J. Phys. Chem. C* **111**, 15337 (2007).
- [42] M. K. Alam, F. Ahmed, R. Miura, A. Suzuki, H. Tsuboi, N. Hatakeyama, A. Endou, H. Takaba, M. Kubo, and A. Miyamoto, *Catal. Today* **164**, 9 (2011).
- [43] Z. Yang, Q. Wang, S. Wei, D. Ma, and Q. Sun, *J. Phys. Chem. C* **114**, 14891 (2010).
- [44] J. Paier, C. Penschke, and J. Sauer, *Chem. Rev.* **113**, 3949 (2013).
- [45] G. Kresse and J. Furthmüller, *Phys. Rev. B* **54**, 11169 (1996).
- [46] P. E. Blöchl, *Phys. Rev. B* **50**, 17953 (1994).
- [47] J. P. Perdew, K. Burke, and M. Ernzerhof, *Phys. Rev. Lett.* **77**, 3865 (1996).
- [48] P. W. Tasker, *Solid State Phys.* **12**, 4977 (1979).
- [49] H. J. Monkhorst and J. D. Pack, *Phys. Rev. B* **13**, 5188 (1976).
- [50] G. Makov, M. C. Payne, *Phys. Rev. B* **51**, 4014 (1995).
- [51] J. Neugebauer, M. Scheffler, *Phys. Rev. B* **46**, 16067 (1992).
- [52] M. Dion, H. Rydberg, E. Schröder, D. C. Langreth, B. I. Lundqvist, *Phys. Rev. Lett.* **92**, 246401 (2004).
- [53] J. Klimeš, D. R. Bowler, and A. Michaelides, *J. Phys.: Condens. Matter* **22**, 022201 (2010); J. Klimeš, D. R. Bowler, and A. Michaelides, *Phys. Rev. B* **83**, 195131 (2011).
- [54] S. Nosé, *J. Chem. Phys.* **81**, 511 (1984); S. Nosé, *Prog. Theor. Phys. Suppl.* **103**, 1 (1991).
- [55] G. Henkelman, B. Uberuaga, H. Jonsson, *J. Chem. Phys.* **113**, 9901 (2000).
- [56] K. Sohlberg, S. T. Pantelides, and S. J. Pennycook, *J. Am. Chem. Soc.* **123**, 6609 (2001).